

Unusual anisotropic response of the charge carrier mobility to uniaxial mechanical strain in Rubrene crystals

Tobias Morf,^{*} Thomas Mathis,[†] and Bertram Batlogg[‡]
Laboratory for Solid State Physics, ETH Zurich, 8093 Zurich, Switzerland
 (Dated: June 29, 2016)

Charge transport in Rubrene single crystals under uniaxial mechanical strain is systematically investigated in the crystal's two in-plane transport directions both under tensile and compressive strain applied parallel or perpendicular to the current direction. The density of trap states remains unchanged. The field-effect mobility as a benchmark figures for intermolecular transport is found to increase with compressive strain and vice versa with a magnitude of $-1.5 \text{ cm}^2 \text{ V}^{-1} \text{ s}^{-1}$ per % of strain independently of transport direction. A very remarkable result is the mobility change when the crystal is strained perpendicular to the transport direction. While this enhancement could be quantitatively explained from an improved wave-function overlap, mobility in the perpendicular direction improves even more, contrary to simple geometric considerations based on lateral expansion and usual Poisson ratios. This result emphasises the central role of the stress induced variations of the dynamics wave function overlap in organic molecular crystals.

Keywords: SINGLE-CRYSTAL; TRANSPORT; MOBILITY; ORGANIC SEMICONDUCTOR; FLEXIBLE; ANISOTROPY; TRAP STATE

I. INTRODUCTION

One of the main applications for organic semiconductors would be flexible electronics. In such devices, the semiconductor will be subject to mechanical strain and it is therefore paramount to understand the effects of strain on the device properties. Furthermore, this question is of fundamental interest for charge transport in organic semiconductors. The building blocks of an organic crystal are extended molecules with richly structured electronic wave functions. These orbitals are spatially highly structured including multiple nodes and lobes^{1–3}. Relatively small displacements are thus expected to cause drastic modifications of the transfer integral and thus charge transport.

Given such an intricate dependence on geometric modifications, it appears highly desirable to study charge transport in single crystals. Furthermore of interest are variations of transport parallel and perpendicular to the applied tensile and compressive strain and along the principal crystallographic directions. Such detailed measurements are an essential extension of previously reported results^{4–10}, mainly on thin film devices which might also reveal effects of grain boundaries and non-uniform crystallite orientation.

II. EXPERIMENT

Organic molecular crystals tend to be fragile and therefore precautions are required when applying mechanical stress. Field-effect transistors were therefore fabricated on flexible PEN foils^{11,12,13} and compressive or tensile strain exerted by bending the foil as shown in fig. 1. Strain at the interface is only a function of bending radius R and amounts to $\varepsilon = \frac{t}{2R}$ where t is the foil thickness. The electrodes, Cytop insulator¹⁴ and $\sim 1 \mu\text{m}$

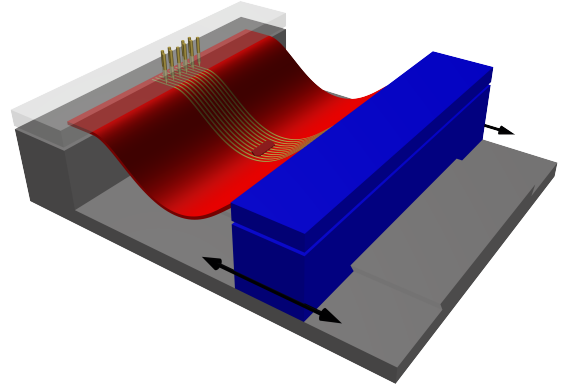


FIG. 1. (Colour online) Illustration of the setup for transistor bending similar to a vice jaw. The substrate (red) with pre-fabricated transistors is clamped to the jaws and the bending radius set by adjusting the position of one jaw (blue). Electrical contact is made through pins in the fixed jaw.

thick Rubrene crystal contribute with the third power of thickness to the total bending moment^{15–17} and are thus negligible compared to the $t = 125 \mu\text{m}$ thick substrate.

For a continuous and controlled setting of the bending radius a vice-like setup was built (fig. 1). Here the substrate is clamped to the jaws, with spring-loaded pins on one jaw making the electrical connections. The distance between the jaws was adjusted by a threaded rod. At well-defined bending radii corresponding to strain values between -0.8% (compressive) and 0.5% (tensile) field-effect transistor (FET) transfer characteristics were measured.

Since the wave function overlap depends on the intermolecular distance and the field effect mobility μ is a

measure of the overlap it is thus expected to sensitively depend on the strain state of the transistor. Apart from purely geometric considerations mechanical strain may also influence the trap density of states (DOS) through mechanical damage. This information can be obtained from the subthreshold region of the transistor¹⁸. In the following, we will therefore discuss the strain-related variations of the mobility in the linear regime μ_{lin} as well as the turn-on V_{on} and threshold voltage V_{th} . Since the turn-on voltage is characterised by the emerging from the noise level and thus depends on the experimental setup, and to reduce experimental scatter, V_{on} was defined at four different current levels well above the noise in the off-state (10 pA, 30 pA, 100 pA and 300 pA). A shift $\Delta V_{\text{on}} > 0$ signifies a shift to more positive voltages, i.e. to the right side in fig. 2 where the p -type Rubrene transistor is in the off state.

III. RESULTS AND DISCUSSION

For both the mobility and the turn-on voltage, the response to externally applied strain usually consists of an irreversible part and a reversible one which is interpreted as damage and elastic changes, respectively. While damage always results in lower mobilities and a shift to the off-state the elastic trend goes in both directions depending on the sign of the strain. Fig. 2 shows the FET transfer characteristics: mobility decreases with tensile strain and increases with compressive strain. Similarly, the turn-on shifts to positive voltages with compressive strain and vice versa.

The measurement protocol involves in general several cycles of compressive and tensile strain over the course several days. Turn-on voltages and corresponding strain values for a typical sample are shown as a timeline in fig. 3. The transistors' turn-on voltage reacts to the application and relaxation of strain in a largely reversible way by shifting $\approx -0.2 \text{ V } \%^{-1}$ and it does so reproducibly and repeatedly over several days in addition to a small, non-recovering shift ascribed to damage. This trend is generally observed in all the crystals shown in fig. 4.

We may express the V_{on} shift in terms of additional charges at the semiconductor-dielectric interface because the shift associated with compression does not only move the turn-on in the direction of the off-state, but actually into the positive gate voltage range. A shift of 0.2 V at -1% (compressive) strain corresponds to an interface charge density of $0.2 \text{ V} \cdot 3.7 \text{ nF cm}^{-2} / e = 5 \times 10^9 \text{ cm}^{-2}$. With the unit cell parameters $a = 14.24 \text{ \AA}$, $b = 7.17 \text{ \AA}$ and two layers of two molecules per unit cell, this translates to two new holes in 10^5 interface molecules.

Remarkably, the shift of V_{on} follows the sign change of the strain, suggesting it to be not simply caused by a mechanical modification of the crystal surface. Upon closer inspection, the V_{on} shift reflects a shift of the entire transfer curve. In fig. 5 ΔV_{on} and ΔV_{th} are shown to follow a strain cycle quantitatively in the same way. The

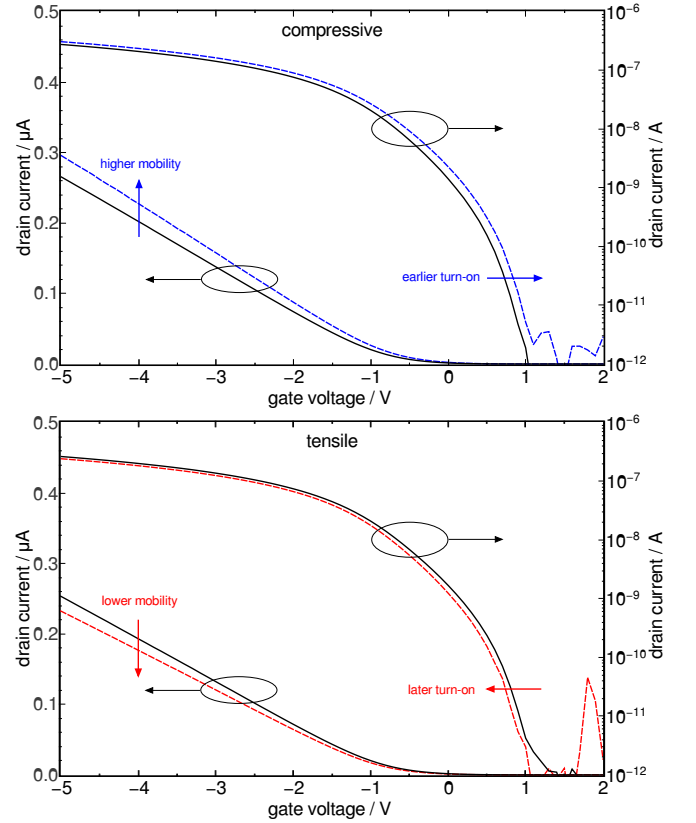


FIG. 2. (Colour online) Transfer characteristics on a linear (left) and logarithmic (right) scale. The black, solid curves represent the relaxed state. Under compressive strain (top panel) the mobility increases and the turn-on voltage shifts to the right (blue, dashed lines). Vice versa for tensile strain (bottom panel) where μ increases and V_{on} shifts to the left (red, dashed lines).

threshold voltage V_{th} , the turn-on voltage V_{on} as well as the four defining voltages for V_{on} are shifted by the same amount. This means that the entire subthreshold region is shifted and thus the deep trap density¹⁸ remains unchanged on the level of $10^{15} \text{ cm}^{-3} \text{ eV}^{-1}$.

Similarly surprising are the strain effects on the charge dynamics, measured in terms of the hole mobility μ_{lin} . The timeline is again shown for four complete strain cycles in fig. 6. The mobility always follows the curve of the applied strain and we observe visible cracks accounting for a reduction of the effective channel width and hence for the overall trend to lower values of the apparent mobility. The changes $\Delta\mu/\epsilon$ do not depend on the initial value of μ_{lin} and amount to approximately $-1.5 \text{ cm}^2 \text{ V}^{-1} \text{ s}^{-1} \%^{-1}$ as shown in fig. 7 on nine transistors. Within the scatter of the data, the crystal's a - and b -directions respond similarly.

A notable exception to the general trend is transistor *1402s* in fig. 7. With $\Delta\mu/\epsilon \approx -5.6 \text{ cm}^2 \text{ V}^{-1} \text{ s}^{-1} \%^{-1}$ it reacts much stronger to the applied strain. Despite this being only one sample, the data are considered very reliable since the transistor is of high quality and

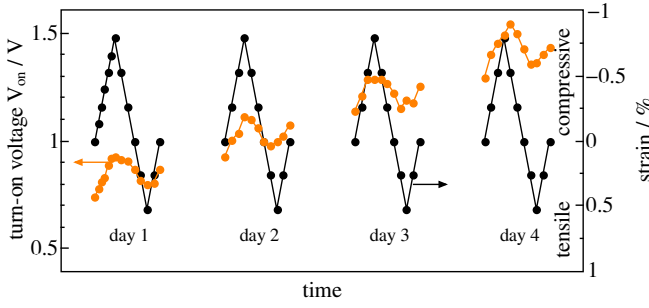


FIG. 3. (Colour online) Typical measurement protocol (black) and corresponding turn-on voltage (orange). One cycle consists of crystal compression, relaxation, tension and relaxation again. At all times, there is a reversible shift going parallel to this curve of applied strain. The overall trend towards higher values of V_{on} is interpreted as damage.

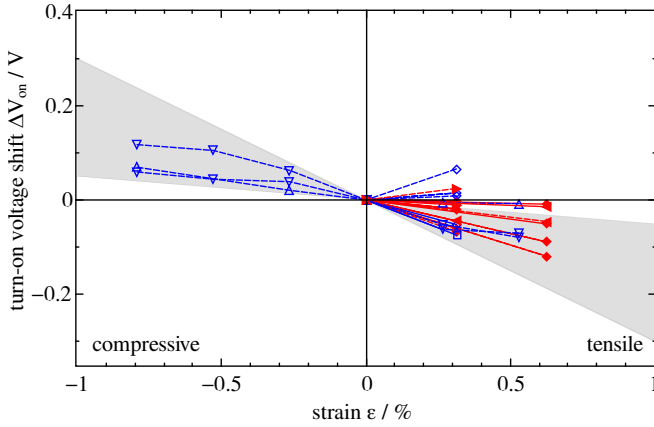


FIG. 4. (Colour online) Summary of turn-on voltage vs. strain of all samples, coloured according to crystallographic transport direction. Blue: a -axis, red: b -axis transport. Within the scatter of the data, there is not visible difference between the two transport directions nor between parallel and perpendicular strain (solid and dashed lines, respectively).

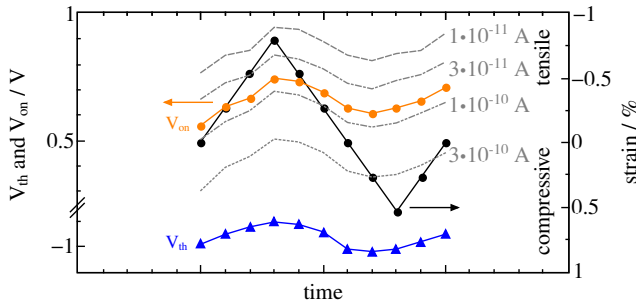


FIG. 5. (Colour online) Threshold and turn-on voltage as a function of applied strain. The four gray curves for V_{on} are averaged to give the orange one. All curves are parallel meaning that the entire subthreshold region is shifted uniformly without affecting the subthreshold slope. This indicates that no new deep trap states are created by mechanical strain.

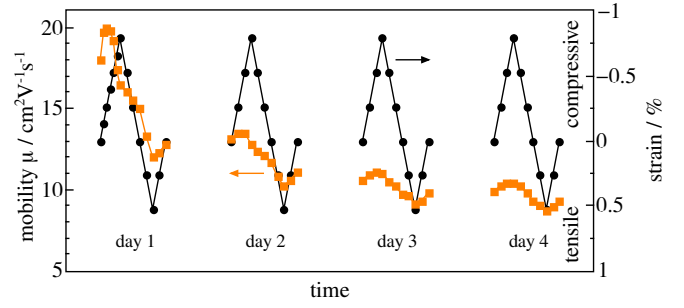


FIG. 6. (Colour online) Typical measurement protocol (black) and corresponding mobility values (orange) on four consecutive days. As for the turn-on voltage, the mobility follows the strain curve in a reversible way indicating an elastic response of the crystal to strain with an associated variation of the molecular orbital overlap. The decreasing trend is attributed to non-elastic, irreversible damage, i.e. cracks effectively reducing the FET channel geometry.

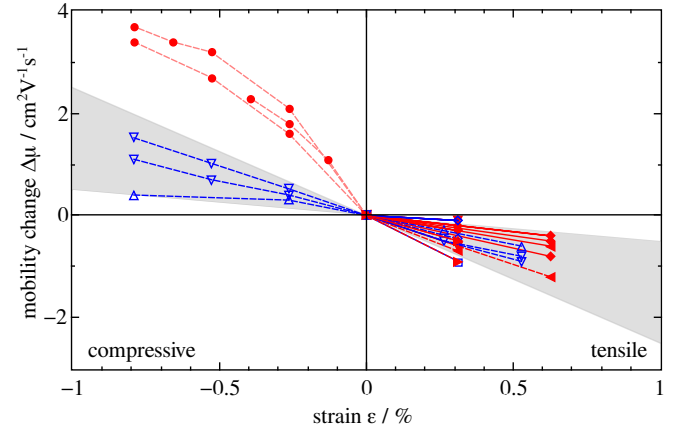


FIG. 7. (Colour online) Summary of mobility vs. strain of all samples, coloured according to crystallographic transport direction as in fig. 4. The general trend for the elastic response is $\approx -1.5 \text{ cm}^2 \text{ V}^{-1} \text{ s}^{-1} \%^{-1}$. One crystal lies well above this range and is therefore considered the upper limit for elastic behaviour due to the absence of visible cracks in the crystal.

the characteristics are very reproducible over multiple strain cycles. The high mobility in the unstrained state of $25 \text{ cm}^2 \text{ V}^{-1} \text{ s}^{-1}$ remains constant within less than $1 \text{ cm}^2 \text{ V}^{-1} \text{ s}^{-1}$ and the crystal does not show any visible cracks in the FET channel area. The very pronounced reaction to mechanical strain can thus be understood as an upper limit to the purely elastic response.

The over-all relatively large influence of strain on the mobility reflects the modification of wave function overlap due to modified relative geometric arrangement and of the dynamics of the molecule. A first, over-simplified estimate would only consider compression of the lattice, i.e. bringing the molecules closer together without any additional slipping or rotating. Such an estimate would result in an increase of the overlap by $\approx 10 \%$ per 1% distance reduction¹ and is consistent with the above mea-

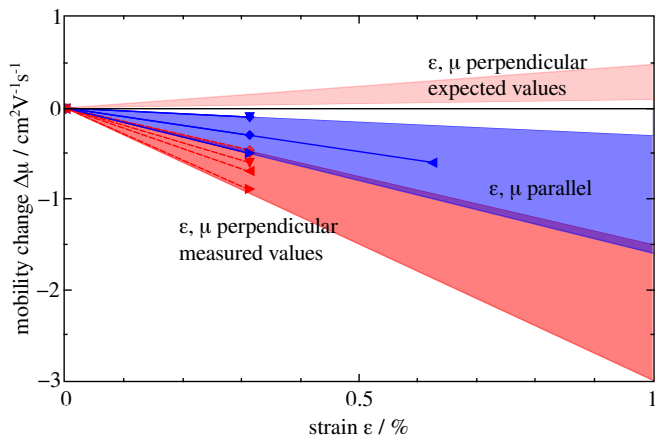


FIG. 8. (Colour online) Mobility change $\Delta\mu/\epsilon$ for five crystals measured with strain parallel to the transport direction (blue) and perpendicular (red). Contrary to the expectation from Poisson's law (light red wedge above $\Delta\mu = 0$, the absolute values are higher in the perpendicular configuration and they have the same sign as the parallel ones.

sured value of $\Delta\mu/\epsilon \approx -1.5 \text{ cm}^2 \text{ V}^{-1} \text{ s}^{-1} \%^{-1}$ for both compressive and tensile strain.

Unexpected and unusual effects are observed then current flows perpendicular to the strain direction. To eliminate extraneous effects, the same transistor was measured in such a way that the strain is either parallel or perpendicular to the current direction. The mobility change of four crystals with current along the b -axis and one along a is shown in fig. 8. In a simple situation, considering only macroscopic geometry, due to lateral contraction and Poisson ratios $\nu \approx 0.3$ one would expect the mobility change with strain perpendicular to transport (top, light red area) to be of opposite sign and lower magnitude compared to the parallel case (blue area). Most remarkably however, in Rubrene, in the perpendicular configuration the mobility response is of the same sign and even larger (bottom, red area) than in the parallel setting. Again, a - and b -axis transport respond similarly.

This unusual response is yet another example of unexpected and nontrivial, anisotropic behaviour of organic molecular crystals after e.g. the observation of thermal contraction in Pentacene¹⁹. While thermal expansion/contraction is a strictly structural effect, our data reveal that the consequences extend to the electronic properties as well.

IV. CONCLUSION

In a systematic study of Rubrene crystal FETs the charge transport and transfer characteristics have been investigated in all possible parameter combinations: compressive and tensile strain along the two principal crystal directions and current flowing parallel or perpendicular to the strain.

We measured a systematic reversible shift of the essentially unchanged transfer curve by $-0.2 \text{ V} \%^{-1}$ corresponding to two new holes per 10^5 interface molecules. This shift is symmetric for tensile and compressive strain and no dependence on the transport direction in the crystal was found. It suggests only minimal deep trap creation but variations in the effective potential at the semiconductor-dielectric interface.

The charge carrier mobility responds in an unexpected and anisotropic way to the applied strain. The general trend of $-1.5 \text{ cm}^2 \text{ V}^{-1} \text{ s}^{-1} \%^{-1}$ is also symmetric, independent of the transport direction and in line with simple estimates based on transfer integral variations upon intermolecular distance change. However, the difference between strain applied parallel and perpendicular to current is most remarkable. If tensile strain is applied perpendicular to the transport direction, the crystal's mobility drops and it does so even stronger than for parallel tensile strain. Both qualitatively and quantitatively, this is at odds with simple geometrical considerations involving lateral contraction.

This is an example of unexpected, anisotropic behaviour of organic single crystals reminiscent of negative thermal expansion in Pentacene single crystals¹⁹. Apart from macroscopic geometric effects, the electronic structure is particularly sensitive to the relative alignment of the molecules due to their highly structured wave functions and the dynamic modulation of their overlap^{1,20–24}. In a unique way the charge mobility is determined by the subtle interplay between quantum localisation on a short timescale due to electronic disorder (both of diagonal and mainly off-diagonal nature) and the subsequent diffusive delocalisation driven by lattice dynamics (for an updated summary, see e.g. ref. 20).

Thus our results stimulate a multitude of further detailed studies of geometry and dynamics of the molecular arrangement under various stress conditions. This will be a challenge for computational and experimental approaches.

ACKNOWLEDGMENTS

Kurt Mattenberger is gratefully acknowledged for technical support.

* tmorf@phys.ethz.ch

† mathis@phys.ethz.ch

- [‡] batlogg@phys.ethz.ch
- ¹ J. Brédas, J. Calbert, da Silva Filho D.A., and J. Cornil, Proc. Natl. Acad. Sci. U. S. A. **99**, 5804 (2002).
 - ² D. da Silva Filho, E.-G. Kim, and J.-L. Brédas, Adv. Mater. **17**, 1072 (2005).
 - ³ V. Coropceanu, J. Cornil, D. A. da Silva Filho, Y. Olivier, R. Silbey, and J.-L. Brédas, Chem. Rev. **107**, 926 (2007).
 - ⁴ T. Sekitani, Y. Kato, S. Iba, H. Shinaoka, T. Someya, T. Sakurai, and S. Takagi, Appl. Phys. Lett. **86**, 073511 (2005).
 - ⁵ M. Kanari, M. Kunitomo, T. Wakamatsu, and I. Ihara, Thin Solid Films **518**, 2764 (2010).
 - ⁶ T. Someya, T. Sekitani, S. Iba, Y. Kato, H. Kawaguchi, and T. Sakurai, Proc. Natl. Acad. Sci. U. S. A. **101**, 9966 (2004).
 - ⁷ D.-K. Lee, S.-C. Lee, Y.-G. Seol, J.-H. Ahn, N.-E. Lee, and Y.-J. Kim, J. Nanosci. Nanotechnol. **11**, 239 (2011).
 - ⁸ F.-C. Chen, T.-D. Chen, B.-R. Zeng, and Y.-W. Chung, Semicond. Sci. Technol. **26**, 034005 (2011).
 - ⁹ K. Sakai, Y. Okada, S. Kitaoka, J. Tsurumi, Y. Ohishi, A. Fujiwara, K. Takimiya, and J. Takeya, Phys. Rev. Lett. **110**, 096603 (2013).
 - ¹⁰ A. L. Briseno, R. J. Tseng, M.-M. Ling, E. H. Falcão, Y. Yang, F. Wudl, and Z. Bao, Adv. Mater. **18**, 2320 (2006).
 - ¹¹ K. Nakayama, W. Ou-Yang, M. Uno, I. Osaka, K. Takimiya, and J. Takeya, Org. Electron. **14**, 2908 (2013).
 - ¹² Y. Kato, S. Iba, T. Termoto, T. Sekitani, T. Someya, H. Kawaguchi, and T. Sakurai, Appl. Phys. Lett. **84**, 3789 (2004).
 - ¹³ Teonex Q65HA was kindly provided by Prof. Jun Takeya's group at Chiba University.
 - ¹⁴ W. L. Kalb, F. Meier, K. Mattenberger, and B. Batlogg, Phys. Rev. B: Condens. Matter Mater. Phys. **76**, 184112 (2007).
 - ¹⁵ J. Case, A. Chilver, and C. Ross, *Strength of Materials and Structures*, fourth edition ed. (Elsevier, 1999).
 - ¹⁶ Z. Suo, E. Ma, H. Gleskova, and S. Wagner, Appl. Phys. Lett. **74**, 1177 (1999).
 - ¹⁷ C.-J. Chiang, C. Winscom, S. Bull, and A. Monkman, Org. Electron. **10**, 1268 (2009).
 - ¹⁸ B. Blülle, R. Häsermann, and B. Batlogg, Phys. Rev. Appl. **1**, 034006 (2014).
 - ¹⁹ S. Haas, B. Batlogg, C. Besnard, M. Schiltz, C. Kloc, and T. Siegrist, Phys. Rev. B: Condens. Matter Mater. Phys. **76**, 205203 (2007).
 - ²⁰ S. Fratini, D. Mayou, and S. Ciuchi, Adv. Funct. Mater. **26**, 2292 (2016).
 - ²¹ A. Troisi and G. Orlandi, J. Phys. Chem. A **110**, 4065 (2006).
 - ²² A. Troisi and G. Orlandi, Phys. Rev. Lett. **96**, 086601 (2006).
 - ²³ A. Troisi, Adv. Mater. **19**, 2000 (2007).
 - ²⁴ J. P. Sleigh, D. P. McMahon, and A. Troisi, Applied Physics A: Materials Science & Processing **95**, 147 (2009).